AD-A162 043 MECHANISMS FOR EXCITED NEUTRALS AND NEGATIVE AND POSITIVE ION DESORPTION F (U) GEORGE WASHINGTON UNIV WASHINGTON D C DEPT OF CHEMISTRY D E RAMAKER OCT 85 1/1

UNCLASSIFIED TR-18 N00014-80-K-0852 F/G 7/5 NL

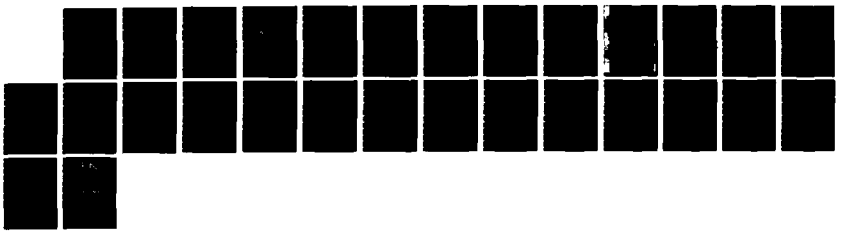

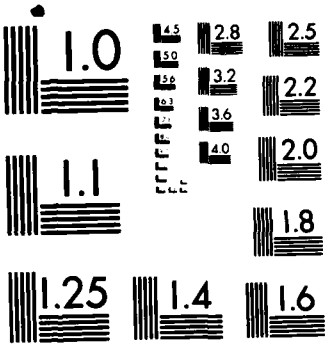

Unclassified
SECURITY CLASSIFICATION OF THIS PAGE (When Data Entered)

REPORT DOCUMENTATION PAGE		READ INSTRUCTIONS BEFORE COMPLETING FORM
1. REPORT NUMBER: No. 18	2. GOVT ACCESSION NO.	3. RECIPIENT'S CATALOG NUMBER
4. TITLE (and Subtitle): MECHANISMS FOR EXCITED NEUTRALS AND NEGATIVE AND POSITIVE ION DESORPTION FROM SURFACES		5. TYPE OF REPORT & PERIOD COVERED: Technical Report 6. PERFORMING ORG. REPORT NUMBER
7. AUTHOR(s): David E. Ramaker		8. CONTRACT OR GRANT NUMBER(s): N00014-80-K-0852
9. PERFORMING ORGANIZATION NAME AND ADDRESS: Chemistry Department, George Washington University, Washington, D.C. 20052		10. PROGRAM ELEMENT, PROJECT, TASK AREA & WORK UNIT NUMBERS: Prog. Elem. No. 61153N, Task Area No. PP 013-08-01, Work Unit # NR 056-681
11. CONTROLLING OFFICE NAME AND ADDRESS: Office of Naval Research, Dept. of Navy, 800 N. Quincy Street, Washington, D.C. 22217		12. REPORT DATE: Oct. 1985 13. NUMBER OF PAGES: 8
14. MONITORING AGENCY NAME & ADDRESS(if different from Controlling Office)		15. SECURITY CLASS. (of this report): Unclassified 15a. DECLASSIFICATION/DOWNGRADING SCHEDULE

16. DISTRIBUTION STATEMENT (of this Report)

This document has been approved for public release and sale; its distribution is unlimited.

17. DISTRIBUTION STATEMENT (of the abstract entered in Block 20, if different from Report)

18. SUPPLEMENTARY NOTES

Submitted for publication in Desorption Induced by Electronic Transitions, DIET II, Springer Verlag.

19. KEY WORDS (Continue on reverse side if necessary and identify by block number)

Photon stimulated desorption; photo-dissociation; fragmentation; electron stimulated desorption; dissociative attachment.

20. ABSTRACT (Continue on reverse side if necessary and identify by block number)

In this review we summarize and generalize the results of a recent detailed comparative investigation of OH^*, OH^+, and H^+ desorption from OH/TiO_2, $H_2O(s)$, and $H_2O(g)$, and O^- and O^+ desorption from O/W and O/Mo(10). Two mechanisms for O^- and OH^* desorption have been proposed which were not revealed in the positive ion desorption yields. These additional electron attachment mechanisms are placed in the context of the previously proposed ionic desorption mechanisms and are discussed in detail.

DD FORM 1 JAN 73 1473 EDITION OF 1 NOV 65 IS OBSOLETE
S/N 0102-014-6601

Unclassified
SECURITY CLASSIFICATION OF THIS PAGE (When Data Entered)

DISCLAIMER NOTICE

THIS DOCUMENT IS BEST QUALITY PRACTICABLE. THE COPY FURNISHED TO DTIC CONTAINED A SIGNIFICANT NUMBER OF PAGES WHICH DO NOT REPRODUCE LEGIBLY.

OFFICE OF NAVAL RESEARCH

N00014-80-K-0852

Task No. 056-681

Technical Report No. 18

MECHANISMS FOR EXCITED NEUTRALS AND NEGATIVE AND POSITIVE ION DESORPTION FROM SURFACES

By

David E. Ramaker

Prepared for Publication

in

Desorption Induced by Electronic Transitions, DIET II,
Springer Verlag

George Washington University
Department of Chemistry
Washington, D.C. 20052

October 1985

21

(1)

Desorption Induced by Electronic Transitions
DIET II

Proceedings of the Second International Workshop,
Schloß Elmau, Bavaria, October 15–17, 1984

Editors: W. Brenig and D. Menzel

With 164 Figures

Springer-Verlag
Berlin Heidelberg New York Tokyo

Mechanisms for Excited Neutral and Negative and Positive Ion Desorption from Surfaces

David E. Ramaker

Department of Chemistry, George Washington University, Washington, DC 20052, USA

1. Introduction

Previous work in electron/photon stimulated desorption (ESD/PSD), utilizing a variety of experimental and theoretical tools, has provided considerable progress towards our understanding of the desorption of ions from covalent systems [1-3]. Comparative investigations of dissociation processes in gas phase, condensed (solid), and chemisorbed systems (e.g.,CO(g), CO(s), and CO/Ru (001), or H_2O(g), H_2O(s), and OH/Ti) have been very helpful in understanding the desorption of ions from molecularly chemisorbed systems [4,5]. Identification of the excited ionic states responsible for the dissociation or desorption, which can often be made by comparison with photoemission and electron-electron coincidence data, reveals that they possess widely different electronic character and hence arise from widely different excitation mechanisms [4,5].

More recently the experimental emphasis has been on the desorption of excited neutrals (X^*), ground state neutrals (X°), and negative ions (X^-) rather than positive ions (X^+). In general, it is believed that the neutral yields (X^* and/or X°) far outnumber the ionic yield (X^+) [1,2], but the relationship between the X^*, X°, X^-, and X^+ desorption mechanisms is not yet clear. Recent data for CO° from CO/Ru suggest the CO° arises from reneutralization, but that CO^* from CO/Ru arises from a direct mechanism (i.e., one of the models in Table 1) [6]. This suggests that CO° and CO^+ yield spectra should be similar, but perhaps different from CO^*. The kinetic energy distribution for H^* (specifically H(2s))desorbed from H_2O(s) (i.e., ice) is significantly different from that for H^+ suggesting a different mechanism for the H^* desorption [7]. The OH^* yield from OH/TiO_2 has additional contributions at low energy which are not observed in the OH^+ yield indicating several different mechanisms are involved in the OH^* desorption [8]. Finally, data on the O^- yield spectra from O/Mo and O/W suggested a resonant electron attachment like process [9].

In this review we shall summarize and generalize the results of a recent detailed comparative investigation of OH^*, OH^+, and H^+ desorption from OH/TiO_2, H_2O(s), and H_2O(g), and O^- and O^+ desorption from O/W and O/Mo [10]. Two mechanisms for O^- and OH^* desorption have been proposed which were not revealed in the positive ion desorption yields. These additional electron attachment mechanisms are placed in the context of the previously proposed

Mechanisms for Excited Neutral and Negative and Positive Ion Desorption from Surfaces

David E. Ramaker

Department of Chemistry, George Washington University, Washington, DC 20052, USA

1. Introduction

Previous work in electron/photon stimulated desorption (ESD/PSD), utilizing a variety of experimental and theoretical tools, has provided considerable progress towards our understanding of the desorption of ions from covalent systems [1-3]. Comparative investigations of dissociation processes in gas phase, condensed (solid), and chemisorbed systems (e.g., CO(g), CO(s), and CO/Ru (001), or H_2O(g), H_2O(s), and OH/Ti) have been very helpful in understanding the desorption of ions from molecularly chemisorbed systems [4,5]. Identification of the excited ionic states responsible for the dissociation or desorption, which can often be made by comparison with photoemission and electron-electron coincidence data, reveals that they possess widely different electronic character and hence arise from widely different excitation mechanisms [4,5].

More recently the experimental emphasis has been on the desorption of excited neutrals (X^*), ground state neutrals (X°), and negative ions (X^-) rather than positive ions (X^+). In general, it is believed that the neutral yields (X^* and/or X°) far outnumber the ionic yield (X^+) [1,2], but the relationship between the X^*, X°, X^-, and X^+ desorption mechanisms is not yet clear. Recent data for CO° from CO/Ru suggest the CO° arises from reneutralization, but that CO^* from CO/Ru arises from a direct mechanism (i.e., one of the models in Table 1) [6]. This suggests that CO° and CO^+ yield spectra should be similar, but perhaps different from CO^*. The kinetic energy distribution for H^* (specifically H(2s))desorbed from H_2O(s) (i.e., ice) is significantly different from that for H^+ suggesting a different mechanism for the H^* desorption [7]. The OH^* yield from OH/TiO_2 has additional contributions at low energy which are not observed in the OH^+ yield indicating several different mechanisms are involved in the OH^* desorption [8]. Finally, data on the O^- yield spectra from O/Mo and O/W suggested a resonant electron attachment like process [9].

In this review we shall summarize and generalize the results of a recent detailed comparative investigation of OH^*, OH^+, and H^+ desorption from OH/TiO_2, H_2O(s), and H_2O(g), and O^- and O^+ desorption from O/W and O/Mo [10]. Two mechanisms for O^- and OH^* desorption have been proposed which were not revealed in the positive ion desorption yields. These additional electron attachment mechanisms are placed in the context of the previously proposed

Table 1 Summary of proposed models for desorption

MODEL	EXCITATION LEVEL	EXCITED STATE	DESORPTION YIELD[a]	APPLICABILITY
MENZEL-GOMER-REDHEAD(MGR)	valence	nhne[b]	X^+, X^*	gas phase dissociation[b] ESD and PSD
ANTONIEWICZ bounce(AB)	valence	1h,1h1e[c]	X^+, X^*	physisorbed gases
KNOTEK-FEIBELMANN(KF)	core	2h	X^+	ionic, maximal valency systems
Auger stimulated desorption(ASD)	core	2h,2h1e	X^+, X^*	covalent and ionic systems, adsorbates
Many particle CI (MPCI)excitations	valence[d]	2h,2h1e	X^+, X^*	covalent systems, adsorbates
Dissociative attachment(DA)	valence	1h2e	X^*, X^-	covalent and ionic systems, adsorbates
e- attachmt.reson. Auger stimultd. desorpt. (RASD)	core	2h2e	X^*, X^-	covalent and ionic systems, adsorbates

[a] During the modification process (step 3), X^c can always result from X^+ via reneutralization.

[b] The final state of the MGR model can be broadly defined as nhne, although sometimes it has been associated with just 1h1e. In the 1h1e case, the MGR mechanism is closely related to the dominant gas phase dissociation mechanism, and it is used in this context in this work. It is applicable to desorption in its broader context. The more specific mechanism, such as those listed below, then provide more insight.

[c] The essence of the AB model involves the initial trajectory of the ion toward the surface where the ion is neutralized (the ANTONIEWICZ "bounce"). Thus the final state could be broadly defined as nhne, although it is often assumed to be 1h1e.

[d] Many particle CI excitations also occur at core levels, but an Auger process usually occurs prior to the desorption (leaving a 3h1e or 3h2e final state) so that it is included in the ASD model.

ionic desorption mechanisms in Table 1 and are discussed in more detail in this review.

The stimulated desorption process can be described approximately as a sequence of three steps [11,2]:
1. a fast initial electronic excitation (10^{-16} sec);
2. decay of the excited state by displacement of the atomic positions but in competition with other electronic decay mechanisms, which redistribute the electronic energy (10^{-15} -10^{-14} sec);
3. a modification (e.g., energy, charge state, etc) of the desorbing species as it recedes from the surface (10^{-14} -10^{-13} sec).

Our knowledge of desorption processes is based, in large part, on examination of the desorbed species: their identities, angular and energy distributions, charge states, and electronic and vibrational energy distributions. All of these quantities can provide clues to the desorption mechanisms, but modifications of the desorbing species (step 3) can obscure the interpretation of the interesting dynamics that occur in step 2.

Most helpful to an elucidation of step 2 has been the careful comparison of PSD spectral data with photoelectron CIS (constant initial state) data or photoabsorption data. This comparison provides insight into the dynamics of step 2 by revealing which initial states eventually result in desorption, and which do not [4,5]. In this context, the possible competitive decay mechanisms are noted, such as Auger decay, autoionization, resonant photoemission, hole delocalization, etc [4,5]. The resultant intermediate excited states can be categorized by the number of "particles" involved, such as one-hole (1h), two-holes (2h), or two-holes plus one-electron (2h1e); indeed the proposed mechanisms to be summarized below can best be described and differentiated in this context [12]. It is important to emphasize that these decay mechanisms are occurring in competition with the atom displacement. Furthermore, only those decay processes which occur within the critical time, t_c, during which the receding atom can still be trapped (i.e., which occur when the atom is within a critical internuclear distance, R_c, where reneutralization and recapture is highly probable) can alter the total desorption cross-section [13]. The processes occurring after t_c are included in step 3. Since generally, the distance R_c is only slightly greater than the equilibrium internuclear distance or bond length, one can discuss the decay mechanisms in terms of states appropriate for the equilibrium atom configurations, and hence they can be probed by normal spectroscopic techniques. A summary of these models is given in Table 1.

The first five of the desorption models listed in Table 1 have been discussed in detail in previous review articles [1-3] so that they will be only briefly described here. The MGR and AB models are not specific as to the exact electronic nature of the excited state, although it is often assumed to be a 1h1e state [2]. The essence of the MGR model is simply that the excited state is repulsive and competition arises between escape and recapture [13]. On the other hand, in the AB model the excited state is attractive providing for a bounce off the surface during which the ion may be neutralized [14]. The AB model appears to be active for physisorbed systems, in particular Xe or Kr/W [15] and N_2O/Ru [6]. The KF model assumes an interatomic Auger decay of a core excitation followed by desorption in a 2h state due to the reversed Madelung potential [16]. The interatomic Auger decay requires a maximal valency ionic system. The ASD model assumes an intraatomic Auger decay of a core hole state followed by desorption via a localized 2h state. Critical to the ASD model is the localization of the 2h state, a condition necessary to provide the Coulomb repulsion for expulsion of the ion [17]. According to configuration interaction theory, localization of the holes in covalent systems results only when the effective hole-hole repulsion U^e is greater than the appropriate covalent interaction V (i.e. $U^e > V$) [18,19]. For highly ionic systems, the KF and ASD

mechanisms become indistinguishable; thus one could consider the ASD mechanism as a generalization or extension of the KF mechanism to covalent systems [2]. The MBCI model includes a valence ionization plus shakeup or shakeoff producing a 2hle or 2h state which is repulsive [4,5]. The repulsive nature of this state may result from the occupation of an antibonding orbital (i.e. the le part) or from the emptying of a bonding orbital (i.e. the 2h part). In any event, the many particle 2hle or 2h state must be long lived.

2. Dissociation of $H_2O(g)$

A comparison of the H^+ and OH^+ PSD spectrum with the H_β and $OH(A\ ^2\Sigma^+)$ ESD spectrum is shown in Fig. 1c. The use of the acronyms PSD and ESD is appropriate for desorption from the solid. More appropriate for the gas phase are the terms photodissociation and electron-ion coincidence spectra, but we shall continue to refer to them as PSD and ESD for convenience (actually, in this case PSD and ESD could refer to photon and electron stimulated dissociation). The excited neutral yields H_β and $OH(A\ ^2\Sigma^+)$ refer to the fluoresence yield of the transition $H(n=4\rightarrow2)$ and $(A\ ^2\Sigma^+\rightarrow X\ ^2\pi)$ respectively as measured by BEENAKKER et al.[20]. The H^+ and OH^+ PSD yields were actually obtained from (e,e+ion) coincidence data reported by TAN et al.[21], but these coincidence data are known to mimic photon excitation.

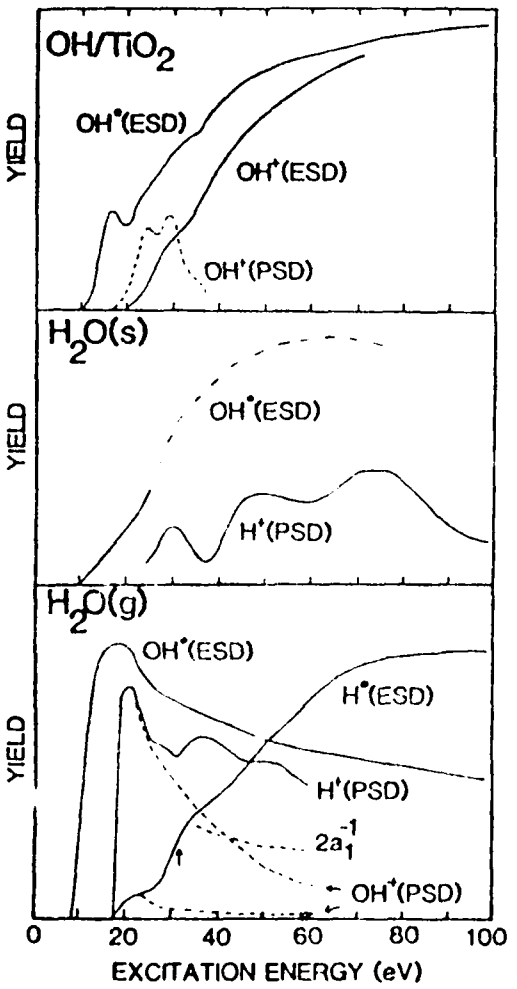

Fig. 1. a) Comparison of the ESD OH^* fluorescence yield $(A\ ^2\Sigma^+ \rightarrow X\ ^2\pi)$ [8], ESD OH^+ ion yield [35], and PSD OH^+ yield [34] from OH/TiO_2. b) Comparison of the ESD OH^* fluorescence yield $(A\ ^2\Sigma^+\rightarrow X\ ^2\pi)$ [29] and PSD H^+ yield [28] from ice. c) Comparison of the ESD H^* fluorescence yield (H_β, $n=4\rightarrow2$) [20], the ESD OH^* fluorescence yield $(A\ ^2\Sigma^+\rightarrow X\ ^2\pi)$ [20], the PSD H^+ ion yield [21], and the PSD OH^+ yield [21] from gas phase H_2O. Also shown is the $2a_1^{-1}$ partial cross-section [21]. The $OH^+(PSD)$, which follows the $1b_1^{-1}$ partial cross-section [21], has been normalized to the $H^+(PSD)$ and $H^*(ESD)$ yields at 23eV. The vertical arrow marks the $2a_1^{-1}$ threshold.

The H^+ and OH^+ PSD spectra have been interpreted in detail previously [4]. The OH^+ yield and the initial peak in the H^+ yield arise from a predissociation of the $1b_2^{-1}$ ionic state. The dissociation must result from a predissociation process, since the $1b_2^{-1}$ potential curve itself is attractive at these energies. The predissociation results from curve crossings with $(1b_1^{-1}\ 3a_1^{-1}\ 4a_1)\ ^2B_1$ and $^4B_1$ states which correlate with the $OH(X\ ^2\Pi) + H^+$ and $OH^+(X\ ^3\Sigma^-) + H$ fragments respectively, giving production of H^+ and OH^+. This 1h mechanism is related to the MGR model in Table 1. The H^+ contributions in the regions 21-25eV and 26-31eV were assigned to the $(1b_1^{-1}\ 3a_1^{-1}\ 4a_1)\ ^2B_1$ and $(1b_1^{-2}\ 4a_1)\ ^2A$ 2hle states [4]. These states derive their intensity from CI mixing with the $1b_1^{-1}$ and $2a_1^{-1}$ 1h states in accordance with the MBCI model in Table 1. The H^+ contribution from 31 to 36eV has been assigned to the $2a_1^{-1}$ excitation, with binding energy at 32eV as indicated by the vertical arrow. The $2a_1^{-1}$ CIS photoelectron yield above 35eV is also shown in Fig. 1c [21]. The exact mechanism for the $2a_1^{-1}$ dissociation process is not known however. Five different dissociation mechanisms have been proposed for this state; they include the ASD, MGR, MBCI mechanisms among others, with the MBCI mechanism favored [4]. Finally an additional H^+ contribution around 47-51eV has been assigned to 2h final states due to ionization plus shakeoff (i.e., the MBCI mechanism).

Careful comparison of the ESD H_β yield with the PSD H^+ yield reveals that the two yields have contributions with similar spectral lineshapes, but with widely different relative intensities. This is somewhat surprising at first since the excitation cross-section of an excited state is expected to be different under electron versus photon excitation. This similarity in lineshape is understandable when one realizes that the H^+ yield comes from photoionization whereas the H_β yield comes from a comparable electron impact excitation into the 4sp Rydberg state [20,22,23]. Thus the 1h, 2h, and 2hle contributions to the PSD H^+ yield correspond to the 1hR, 2hR, and 2hleR excitations (R=Rydberg) in the ESD H_β yield [10]. The reduced size of the 1hR H_β contributions compared to the 1h H^+, and increased size of the 2hR H_β contribution compared to the 2h H^+, may result from either different relative cross-sections and/or different branching ratios for the dissociation processes.

The ESD OH^* yield, as exhibited from the $A\ ^2\Sigma^+ \rightarrow X\ ^2\Pi$ fluorescence yield, has a spectral lineshape similar to the $1b_2^{-1}$ photoionization cross-section, suggesting that the OH^* yield also arises from an electron impact excitation. Detailed polarization dependent studies [24], theoretical studies [25], and product vibrational analysis [26] clearly identify the OH^* yield as resulting from the $3a_1 \rightarrow 4a_1$ electronic excitation (i.e., the MGR mechanism).

3. Desorption from $H_2O(s)$

The PSD H^+ yield from ice shown in Fig. 1b has been previously reported [27,28] and interpreted [4]. The 2hle contributions around 21-35eV and the 2h contributions above 35eV remain. The $1b_2^{-1}$ and $2a_1^{-1}$ 1h contributions disappear, the former because the $1b_2^{-1}$ state delocalizes before the very slow predissociation process has time to occur, the latter presumably because hydrogen

The H^+ and OH^+ PSD spectra have been interpreted in detail previously [4]. The OH^+ yield and the initial peak in the H^+ yield arise from a predissociation of the $1b_2^{-1}$ ionic state. The dissociation must result from a predissociation process, since the $1b_2^{-1}$ potential curve itself is attractive at these energies. The predissociation results from curve crossings with $(1b_1^{-1}\ 3a_1^{-1}\ 4a_1)\ ^2B_1$ and $^4B_1$ states which correlate with the $OH(X\ ^2\Pi) + H^+$ and $OH^+(X\ ^3\Sigma^-) + H$ fragments respectively, giving production of H^+ and OH^+. This 1h mechanism is related to the MGR model in Table 1. The H^+ contributions in the regions 21-25eV and 26-31eV were assigned to the $(1b_1^{-1}\ 3a_1^{-1}\ 4a_1)\ ^2B_1$ and $(1b_1^{-2}\ 4a_1)\ ^2A$ 2hle states [4]. These states derive their intensity from CI mixing with the $1b_1^{-1}$ and $2a_1^{-1}$ 1h states in accordance with the MBCI model in Table 1. The H^+ contribution from 31 to 36eV has been assigned to the $2a_1^{-1}$ excitation, with binding energy at 32eV as indicated by the vertical arrow. The $2a_1^{-1}$ CIS photoelectron yield above 35eV is also shown in Fig. 1c [21]. The exact mechanism for the $2a_1^{-1}$ dissociation process is not known however. Five different dissociation mechanisms have been proposed for this state; they include the ASD, MGR, MBCI mechanisms among others, with the MBCI mechanism favored [4]. Finally an additional H^+ contribution around 47-51eV has been assigned to 2h final states due to ionization plus shakeoff (i.e., the MBCI mechanism).

Careful comparison of the ESD H_β yield with the PSD H^+ yield reveals that the two yields have contributions with similar spectral lineshapes, but with widely different relative intensities. This is somewhat surprising at first since the excitation cross-section of an excited state is expected to be different under electron versus photon excitation. This similarity in lineshape is understandable when one realizes that the H^+ yield comes from photoionization whereas the H_β yield comes from a comparable electron impact excitation into the 4sp Rydberg state [20,22,23]. Thus the 1h, 2h, and 2hle contributions to the PSD H^+ yield correspond to the 1hR, 2hR, and 2hleR excitations (R=Rydberg) in the ESD H_β yield [10]. The reduced size of the 1hR H_β contributions compared to the 1h H^+, and increased size of the 2hR H_β contribution compared to the 2h H^+, may result from either different relative cross-sections and/or different branching ratios for the dissociation processes.

The ESD OH^* yield, as exhibited from the $A\ ^2\Sigma^+ \rightarrow X\ ^2\Pi$ fluorescence yield, has a spectral lineshape similar to the $1b_2^{-1}$ photoionization cross-section, suggesting that the OH^* yield also arises from an electron impact excitation. Detailed polarization dependent studies [24], theoretical studies [25], and product vibrational analysis [26] clearly identify the OH^* yield as resulting from the $3a_1 \rightarrow 4a_1$ electronic excitation (i.e., the MGR mechanism).

3. Desorption from $H_2O(s)$

The PSD H^+ yield from ice shown in Fig. 1b has been previously reported [27,28] and interpreted [4]. The 2hle contributions around 21-35eV and the 2h contributions above 35eV remain. The $1b_2^{-1}$ and $2a_1^{-1}$ 1h contributions disappear, the former because the $1b_2^{-1}$ state delocalizes before the very slow predissociation process has time to occur, the latter presumably because hydrogen

The H^+ and OH^+ PSD spectra have been interpreted in detail previously [4]. The OH^+ yield and the initial peak in the H^+ yield arise from a predissociation of the $1b_2^{-1}$ ionic state. The dissociation must result from a predissociation process, since the $1b_2^{-1}$ potential curve itself is attractive at these energies. The predissociation results from curve crossings with $(1b_1^{-1}\ 3a_1^{-1}\ 4a_1)\ ^2B_1$ and $^4B_1$ states which correlate with the $OH(X\ ^2\Pi) + H^+$ and $OH^+(X\ ^3\Sigma^-) + H$ fragments respectively, giving production of H^+ and OH^+. This 1h mechanism is related to the MGR model in Table 1. The H^+ contributions in the regions 21-25eV and 26-31eV were assigned to the $(1b_1^{-1}\ 3a_1^{-1}\ 4a_1)\ ^2B_1$ and $(1b_1^{-2}\ 4a_1)\ ^2A$ 2hle states [4]. These states derive their intensity from CI mixing with the $1b_1^{-1}$ and $2a_1^{-1}$ 1h states in accordance with the MBCI model in Table 1. The H^+ contribution from 31 to 36eV has been assigned to the $2a_1^{-1}$ excitation, with binding energy at 32eV as indicated by the vertical arrow. The $2a_1^{-1}$ CIS photoelectron yield above 35eV is also shown in Fig. 1c [21]. The exact mechanism for the $2a_1^{-1}$ dissociation process is not known however. Five different dissociation mechanisms have been proposed for this state; they include the ASD, MGR, MBCI mechanisms among others, with the MBCI mechanism favored [4]. Finally an additional H^+ contribution around 47-51eV has been assigned to 2h final states due to ionization plus shakeoff (i.e., the MBCI mechanism).

Careful comparison of the ESD H_β yield with the PSD H^+ yield reveals that the two yields have contributions with similar spectral lineshapes, but with widely different relative intensities. This is somewhat surprising at first since the excitation cross-section of an excited state is expected to be different under electron versus photon excitation. This similarity in lineshape is understandable when one realizes that the H^+ yield comes from photoionization whereas the H_β yield comes from a comparable electron impact excitation into the 4sp Rydberg state [20,22,23]. Thus the 1h, 2h, and 2hle contributions to the PSD H^+ yield correspond to the 1hR, 2hR, and 2hleR excitations (R=Rydberg) in the ESD H_β yield [10]. The reduced size of the 1hR H_β contributions compared to the 1h H^+, and increased size of the 2hR H_β contribution compared to the 2h H^+, may result from either different relative cross-sections and/or different branching ratios for the dissociation processes.

The ESD OH^* yield, as exhibited from the $A\ ^2\Sigma^+ \rightarrow X\ ^2\Pi$ fluorescence yield, has a spectral lineshape similar to the $1b_2^{-1}$ photoionization cross-section, suggesting that the OH^* yield also arises from an electron impact excitation. Detailed polarization dependent studies [24], theoretical studies [25], and product vibrational analysis [26] clearly identify the OH^* yield as resulting from the $3a_1 \rightarrow 4a_1$ electronic excitation (i.e., the MGR mechanism).

3. Desorption from $H_2O(s)$

The PSD H^+ yield from ice shown in Fig. 1b has been previously reported [27,28] and interpreted [4]. The 2hle contributions around 21-35eV and the 2h contributions above 35eV remain. The $1b_2^{-1}$ and $2a_1^{-1}$ 1h contributions disappear, the former because the $1b_2^{-1}$ state delocalizes before the very slow predissociation process has time to occur, the latter presumably because hydrogen

bonding in ice broadens all a_1 bands, allowing for fast delocalization of the $3a_1^{-2}$ $4a_1$ excitation and other repulsive 2hle excitations involving the a_1 orbitals [4].

Although H^* desorption from ice upon electron excitation is believed to have been observed, its spectral lineshape has not been reported in the literature [10,29]. The ESD OH^* yield from ice has been reported from 0 to 25eV as shown in Fig. 1b [29]. Above 25eV, PRINCE et al. [29] describe the spectrum qualitatively without reporting it, thus the dashed line in Fig. 1b is only qualitative.

Comparison of the OH^* yield from $H_2O(g)$ and $H_2O(s)$ reveals a similar threshold, but with a significantly different spectral lineshape. Since a comparison of the $H_2O(g)$ and H_2O (s) absorption spectra reveal similar $3a_1$-$4a_1$ excitations [30], the much slower rise in the OH^* yield from ice in Fig. 1b suggests that the $3a_1^{-1}$ $4a_1$ state is not sufficient to produce OH^* desorption from ice, probably because this 1hle state is not sufficiently long lived (i.e., the MGR mechanism is not active in the condensed phase). The common threshold however suggests that the OH^* yield results primarily from a 1hle $4a_1$ resonant dissociative attachment process (i.e., the DA mechanism listed in Table 1). This many-particle 1h2e type state, similar to that found previously for the 2hle type state, is expected to remain localized longer than the comparable 1hle type state, and thus could be active in the desorption process. This type of resonant process also occurs in gas phase molecules but only contributes to the sharp turn on at threshold [31,32]. In the solid, backscattered and secondary electrons coming from the bulk at all energies lower than the primary energy, may resonantly excite this at all primary energies and make it appear non-resonant. More quantitative data in the future will allow this hypothesis to be tested utilizing a deconvolution procedure [33] which will be summarized below for OH/TiO_2. Stronger conclusions concerning neutral desorption from ice must therefore await further experimental data.

4. Desorption from OH/TiO_2

The OH^+(PSD), OH^+(ESD), and OH^*(ESD) spectra from OH/TiO_2 are compared in Fig. 1a. The OH^+(PSD) spectrum above 35eV is not available, but below 35eV [34] it clearly reveals that the yield from 20-35eV arises from similar 2hle excitations as described above for dissociation of $H_2O(g)$, and as explained by the MPCI model. The initial threshold around 20eV in the OH^+(ESD) [35] is believed to have the same origin.

Similar intramolecular MPCI contributions to the H^+(PSD) yield from OH/Ti (as well as OH/Cr and Cu) have also been reported [28]. However, in the case of these metallic substrates, negligible amounts of OH^+ were seen. Thus from OH/TiO_2, OH^+ and H^+ ions are desorbed, from OH/Ti, Cr, or Cu essentially only H^+ ions are desorbed. This difference between the metallic substrates and the semiconducting TiO_2 substrate probably reflects the increased rate of reneutralization and/or increased rate of delocalization of the 2hle excited states localized in the Ti-O bonds at the metal surface. The H^+ yield from OH/Ti is not eliminated, perhaps

because in this case the 2hle states are more localized on the O-H bond where the metal substrate has a reduced effect.

Above ~37eV, an additional contribution appears in the OH^+(ESD) yield [35]. Initially, it was unclear whether this was due to the $2a_1^{-1}$ intramolecular OH excitation (actually for OH this should be $2\sigma^{-1}$ but we shall continue to refer to it as $2a_1^{-1}$ appropriate for H_2O) or due to the Ti $3p^{-1}$ excitation [36,4]. Again the PSD work on OH/Ti, Cr, and Cu is helpful here, since it reveals H^+ contributions from the metal $3p^{-1}$ excitations for Cr and Cu, with no contribution from the $2a_1^{-1}$ excitations for Cr and Cu [28]. Thus the 32eV threshold in Fig. 1a has been assigned to the Ti $3p^{-1}$ excitation and attributed to the ASD mechanism [10].

The OH^* (in particular the $OH^*(3a_1^{-1}\ 4a_1)$) yield [8] definitely has a lower threshold than OH^+, indeed it agrees with the threshold for OH^* from $H_2O(s)$ and $H_2O(g)$. Consistent with the above interpretation for $H_2O(s)$, it would appear that at least the initial peak around 17eV arises from the DA mechanism. On the other hand, the similarity of the OH^* yield with the OH^+(ESD) yield above 35eV suggests the Ti $3p^{-1}$ ASD mechanism is also active.

The quantitative interpretation of the OH^* yield requires three steps, all of which have been performed previously:

1. the extent of the OH^* yield arising from backscattered and secondary electrons was quantitatively determined [33];
2. the resonant contributions (i.e., the DA and RASD contributions) were separated from the MPCI and ASD contributions [10,33]; and
3. the spectral lineshapes of the $3a_1^{-1}$ and Ti $3p^{-1}$ excitations were determined and compared with the OH^* yield [10].

Step 1 was accomplished by measuring the loss spectrum $L(E_p,\varepsilon)$ at several primary energies E_p. The secondary, $SEC(E_p,\varepsilon)$, and redistributed primary, $RP(E_p,\varepsilon)$ loss contributions were then separated out, and the total yield spectrum measured in order to determine $A(E_p)$ and $B(E_p)$ such that,

$$L(E_p,\varepsilon) = A(E_p)\ SEC(E_p,\varepsilon) + B(E_p)\ RP(E_p,\varepsilon) + ES(E_p), \qquad (1)$$

where $ES(E_p)$ is the elastically scattered peak [33]. The experimental, $N(E)$, and "true", $N_t(E)$, yields are then related by the expression,

$$N(E) = \int L(E_p,\varepsilon)\ N_t(\varepsilon)\ d\varepsilon, \qquad (2)$$

and are given in Fig. 2. Figure 2 shows that about one-third of the yield above 75eV arises from backscattered and secondary electrons, but equally important, it also shows that the major contribution arises from a direct excitation process.

Step 2 above was accomplished by assuming that the total nonresonant ASD and MPCI contributions to OH^* have the same spectral lineshape as the OH^+ yield [10]. This is expected to be true if the OH^* yield arises from either reneutralization of the desorbing OH^+, or more likely if it arises directly via the 2hle excited states within the ASD mechanism. The resonant-nonresonant separation is shown in Fig. 3, where the OH^+ yield was normalized so

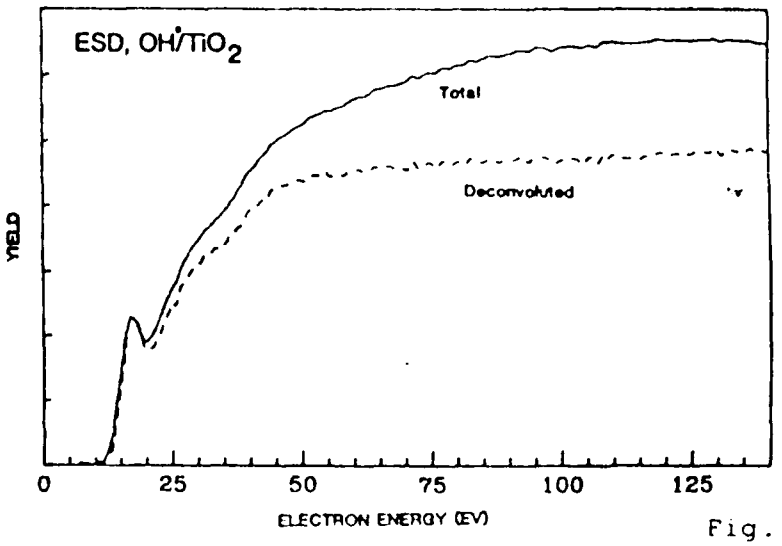

Fig. 2. Comparison of the measured ESD OH^* yield from OH/TiO_2 with the deconvoluted OH^* yield [33].

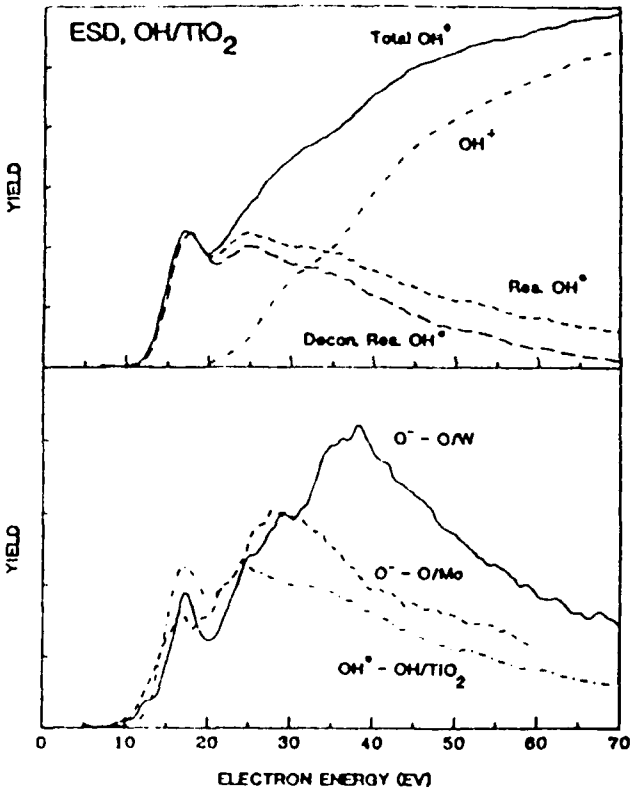

Fig. 3. Top: Comparison of the ESD OH^* yield [8] from OH/TiO_2 with the OH^+ yield [34]. The resonant OH^* yield, as obtained by subtraction of the above two curves, and the deconvoluted resonant OH^* are also shown [33]. Bottom: Comparison of ESD O^- yield from O/W and O/Mo [9] with the resonant OH^* yield from above.

that the deconvoluted resonant OH^* yield went to zero at higher energies.

Finally, estimates of the spectral lineshapes for the $3a_1^{-1}$ and Ti $3p^{-1}$ excitations (i.e., step 3) can be obtained from CIS or EELS (electron energy loss) data. The $3a_1^{-1}$ partial cross-section has been assumed to be similar to the O K EELS spectrum [37] from TiO_2 as shown in Fig. 4. It shows two main features assigned to the $3d^*$ and v^* valence antibonding orbitals in the continuum [38]. Figure 4 shows an estimated separation into the resonant and nonresonant continuum contributions [10]. The DA contribution to the OH^* yield can then be estimated by the self-fold of the

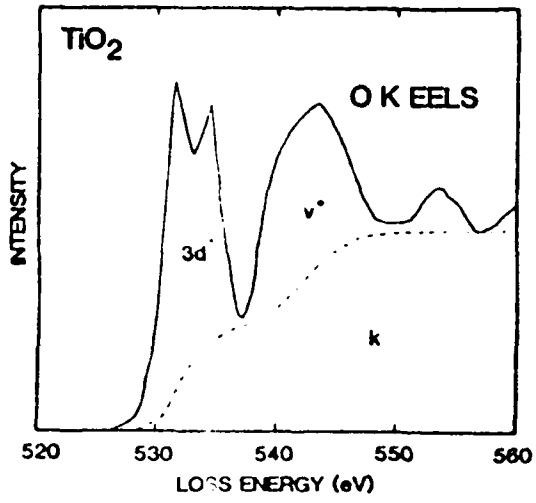

Fig. 4. The O K EELS spectrum [37] from TiO_2 with the $3d^*$ and v^* resonant and the k non-resonant contributions indicated. The k contribution was estimated graphically by the SHIRLEY method [47] and includes all multiple scattering contributions.

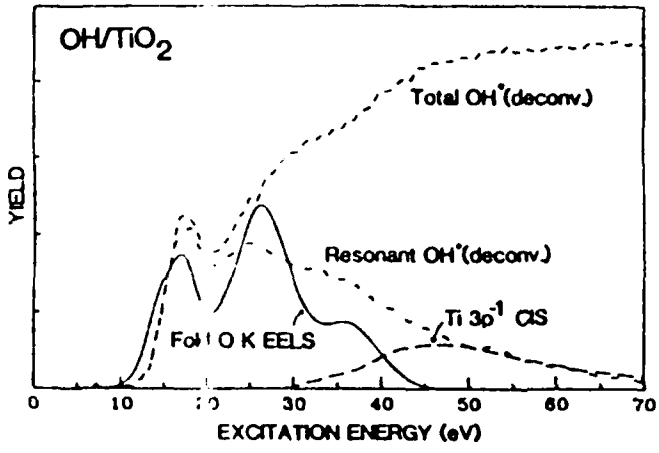

Fig. 5. Comparison of the total deconvoluted $OH^*(A\ ^2\Sigma^+ \rightarrow X\ ^2\Pi)$ yield and the resonant portion of the experimental OH^* yield from OH/TiO_2 [33]. Also shown is the self-fold of the resonant portion of the O K EELS spectrum from Fig. 4 representing the DA contribution, and the Ti $3p^{-1}$ CIS spectrum [10] representing the RASD contribution. The fold of the O K EELS has been positioned for best alignment with the peaks in the OH^* yield.

resonant portion of the O K EELS spectrum representing excitation into the $3a_1^{-1}\ 3d^{*2}$, $3a_1^{-1}\ 3d^*\ v^*$, and $3a_1^{-1}\ v^{*2}$ (1h2e type) states which lead to desorption. This is compared in Fig. 5 with the resonant OH^* yield.

The $3p^{-1}\ 3d^*\ 4a_1$ RASD contribution is approximated in Fig. 5 by the Ti $3p^{-1}$ CIS spectrum [36]. The $3p^{-1}$ spectrum is dominated by the $3p^{-1}\ 3d^*$ excitation, and is known to be very atomic-like due to the large 3p-3d exchange interaction [39]. Because of this atomic-like nature, and because the $4a_1$ valence-like orbital is localized more on the OH absorbate, the $3p^{-1}\ 3d^*\ 4a_1$ excitation is best represented in this case by the straight $3p^{-1}$ CIS spectrum rather than by the self-fold.

The relative magnitudes of the empirical DA and RASD contributions are obtained from the best overall visual fit to the experimental resonant OH^* yield. The excellent fit lends strong support for this interpretive scheme.

Both the DA and RASD mechanisms involve electron attachment resulting in two electrons bound in an antibonding orbital. The DA mechanism involves a valence excitation, generally from a bonding orbital. The small overlap between the bonding and antibond-

ing orbitals allows only a small Auger autoionization decay rate and provides for 1h2e state lifetimes of the order 10^{-10}-10^{-13} sec. in gas phase molecules [32] and similar surprisingly long lifetimes in semiconductors [40]. These states are sufficiently long lived to initiate desorption. They are in contrast to the very short lifetimes (10^{-15}-10^{-16} sec.) observed recently for electron attachment into 1e type shaped resonances in molecular adsorbates on metals [41], which will not initiate desorption. Electron attachment involving excitation from the core orbitals allows for a much faster Auger decay rate, indeed in the Ti 3p case, a very fast super Coster Kronig decay results in a 2h2e type state, if the two electrons remain as a spectator to the Auger decay, as well as 1h1e and 0h0e states (i.e., return to the ground state), if one or both excited electrons are involved in the Auger decay [39]. Of these, the 2h2e type states are sufficiently localized and can result in desorption as described by the RASD mechanism. The relative branching ratios for these various decay processes can be critical to determining the relative magnitudes of the DA, RASD, and ASD processes [42]. The repulsive nature of the 1h2e or 2h2e excited states results from both parts of these excitations (i.e., one or two holes in a bonding orbital and 2 electrons in an antibonding orbital). The many particle nature of these 1h2e states apparently slows the delocalization process in the solid similar to the way it does for the 2h1e and 2h states.

5. Desorption from O/W and Mo

A comparison of the resonant OH^* yield from OH/TiO_2 with the total O^- yield from O/W and O/Mo is shown in Fig. 3. All three spectra show an initial peak around 17eV, a second feature around 22-27eV, a third feature around 33-40eV, and a similar decreasing slope up to 70eV. The np (n=3, 4, and 5 for Ti, Mo, and W respectively) core level in all three metals is around 35eV, and the conduction band density of states (e.g., the O K EELS spectra) is reasonably similar for these transition metal oxides. The similarity of the total O^- yield with the resonant OH^* yield suggests that the O^- yield arises primarily from the resonant DA and RASD processes, which yield 1h2e or 2h2e excited states respectively, while the OH^* yield may occur from 1h2e, 2h2e, and 2h1e excited states, the latter which may result from the non-resonant ASD process.

It was indicated above that the RASD mechanism is active in O^- desorption (and maybe also O neutrals), but it is doubtful that it is active in O^+ desorption. One way to test this is to compare the derivative of the O^+(ESD) yield with the O^+(PSD) yield. Electron attachment can of course occur only in ESD. To first order the ESD spectral lineshape can be approximated by the self-fold of the PSD lineshape [10],

$$ESD(E) = \int PSD(E-\epsilon)\, PSD(\epsilon)\, d\epsilon = PSD \times PSD \,. \qquad (3)$$

The PSD spectral lineshape includes terms resulting from excitation into antibonding resonances (v^*) and into the continuum (k) as shown in Fig. 4, thus;

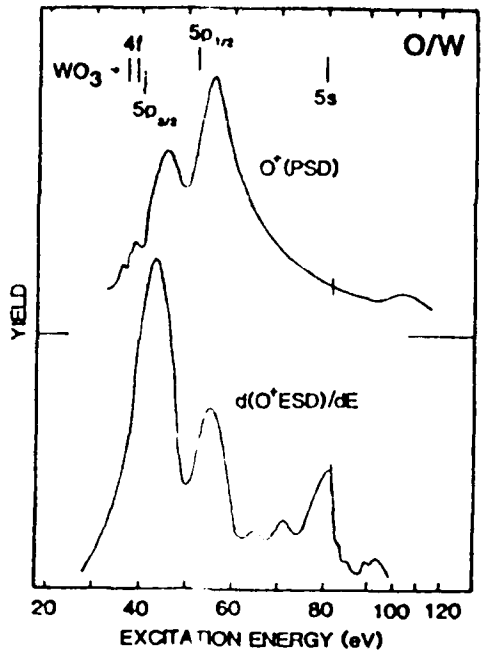

Fig. 6. Comparison of the derivative of the ESD O^+ yield [43] and the PSD O^+ yield [44] from O/W.

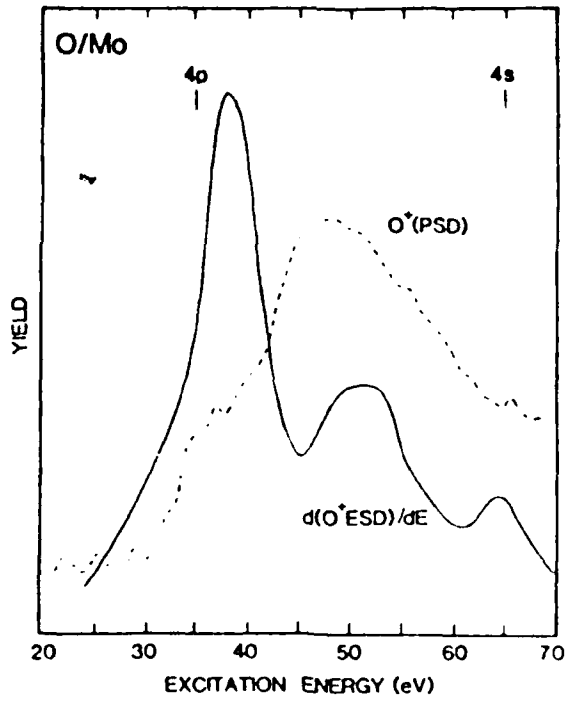

Fig. 7. Comparison of the derivative of the ESD O^+ yield [43] and the PSD O^+ yield [45] from O/Mo.

$$PSD(E) = v^* + k \tag{4}$$

and it follows that

$$ESD(E) = v^* \times v^* + 2v^* \times k + k \times k \ . \tag{5}$$

As shown in Fig. 4, the continuum contribution is relatively slowly varying with energy E (except near threshold) so that,

$$\frac{d(v^* \times 1)}{dE} \propto v^* \quad \text{and} \quad \frac{d(k \times k)}{dE} = \text{constant}, \tag{6}$$

and

$$\frac{dESD(E)}{dE} \approx \frac{d(v^* \times v^*)}{dE} + 2PSD(E) + \text{constant}. \tag{7}$$

The first term above corresponding to electron attachment is highly structured. Its presence or absence in the O^+ ESD spectrum should be evident by comparing d(ESD)/dE [43] with the PSD spectra [44,45] as shown in Figs. 6 and 7 for O^+ from O/W and O/Mo. The similarity in the curves is clearly evident well above each threshold. The large peaks at each threshold (i.e., at the np and ns) in the d(ESD)/dE curves may arise partly from the variation in k near threshold, but more likely result from non-dipole excitations into the continuum [46]. The dipole selection rule valid for photons, is valid only well above threshold for electrons.

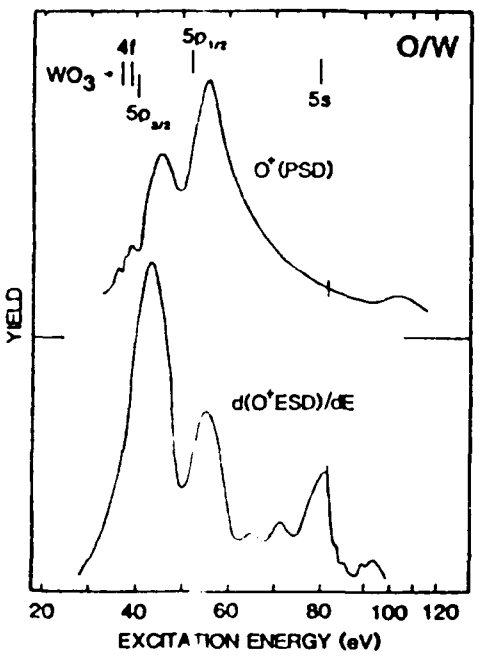

Fig. 6. Comparison of the derivative of the ESD O^+ yield [43] and the PSD O^+ yield [44] from O/W.

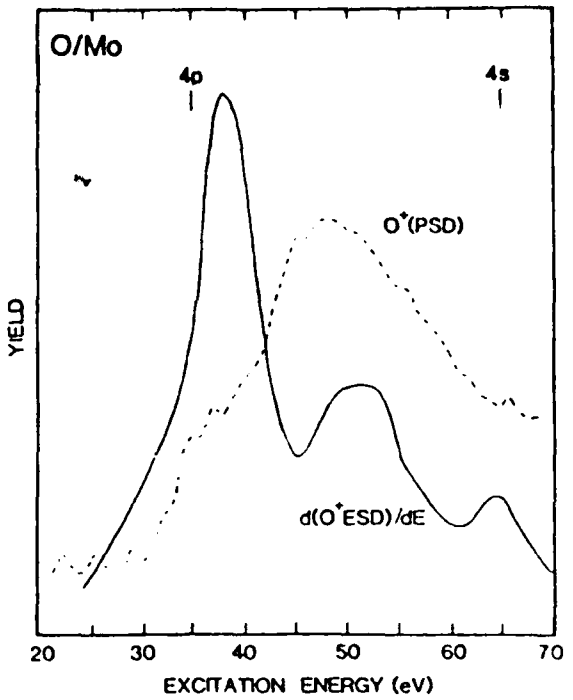

Fig. 7. Comparison of the derivative of the ESD O^+ yield [43] and the PSD O^+ yield [45] from O/Mo.

$$PSD(E) = v^* + k \tag{4}$$

and it follows that

$$ESD(E) = v^* \times v^* + 2v^* \times k + k \times k \ . \tag{5}$$

As shown in Fig. 4, the continuum contribution is relatively slowly varying with energy E (except near threshold) so that,

$$\frac{d(v^* \times v^*)}{dE} \propto v^* \quad \text{and} \quad \frac{d(k \times k)}{dE} = \text{constant}, \tag{6}$$

and

$$\frac{dESD(E)}{dE} = \frac{d(v^* \times v^*)}{dE} + 2PSD(E) + \text{constant}. \tag{7}$$

The first term above corresponding to electron attachment is highly structured. Its presence or absence in the O^+ ESD spectrum should be evident by comparing d(ESD)/dE [43] with the PSD spectra [44,45] as shown in Figs. 6 and 7 for O^+ from O/W and O/Mo. The similarity in the curves is clearly evident well above each threshold. The large peaks at each threshold (i.e., at the np and ns) in the d(ESD)/dE curves may arise partly from the variation in k near threshold, but more likely result from non-dipole excitations into the continuum [46]. The dipole selection rule valid for photons, is valid only well above threshold for electrons.

Table 2 Primary desorption mechanisms assigned for the systems reviewed in this work

SYSTEM	OH^+(ESD/PSD)	OH^*(ESD)	H^*(ESD)	H^+(PSD)
H_2O(g)	MGR	MGR	MGR & MBCI	MGR & MBCI
H_2O(s)	Not obs.	DA[a]	MBCI[a]	MBCI
OH/TiO_2	MBCI & ASD	DA, RASD, MBCI & ASD	Not obs.	MBCI & ASD
		O^-(ESD)	O^+(ESD)	O^+(PSD)
O/M		DA & RASD	ASD	ASD

[a]Data here is sparse, see Ref. [10] for further discussion.

The apparent absence of the resonant electron attachment contributions to the O^+ ESD yield supports the assumption that the RASD mechanism involving the $3p^{-1}$ excitation produces primarily O^- and perhaps O, but little O^+. It also lends support to our resonant-nonresonant separation procedure used above for the OH^* yield from OH/TiO_2.

6. Summary and Conclusions

A summary of the mechanisms involved in the systems reviewed in this work is given in Table 2. Assignments of the specific states responsible for the desorption have been given in the text, and are summarized in more detail elsewhere [10].

Several conclusions can be made based upon the results summarized in this work. They are as follows:

1. In the gas phase, the ESD H^* yield mimics the PSD H^+ yield because electron impact excitation mimics photoionization. However on the surface secondary and backscattered electrons distort this correlation.
2. On the surface, the derivative of the ESD O^+ yield mimics the PSD O^+ yield because the non-resonant ASD mechanism dominates for the O^+ yield. Non-dipole excitations become important near the thresholds.
3. In the DA and RASD mechanisms, the incoming electron provides both the excitation energy and assists in the localization of that energy in the 1h2e and 2h2e states. The photon can only provide for the excitation energy.
4. Secondary and backscattered electrons are important for low threshold desorption processes such as for X^* and X^-, however, the magnitude of this effect in X^+ desorption, where thresholds are higher, is not yet clear.
5. Apparently X^- desorption can result from 1h2e and 2h2e states, X^* from 1h2e, 2h2e, and 2h1e states, and X^+ from 2h1e and 2h

Table 2 Primary desorption mechanisms assigned for the systems reviewed in this work

SYSTEM	OH^+(ESD/PSD)	OH^*(ESD)	H^*(ESD)	H^+(PSD)
H_2O(g)	MGR	MGR	MGR & MBCI	MGR & MBCI
H_2O(s)	Not obs.	DA[a]	MBCI[a]	MBCI
OH/TiO_2	MBCI & ASD	DA, RASD, MBCI & ASD	Not obs.	MBCI & ASD
		O^-(ESD)	O^+(ESD)	O^+(PSD)
O/M		DA & RASD	ASD	ASD

[a]Data here is sparse, see Ref. [10] for further discussion.

The apparent absence of the resonant electron attachment contributions to the O^+ ESD yield supports the assumption that the RASD mechanism involving the $3p^{-1}$ excitation produces primarily O^- and perhaps O, but little O^+. It also lends support to our resonant-nonresonant separation procedure used above for the OH^* yield from OH/TiO_2.

6. Summary and Conclusions

A summary of the mechanisms involved in the systems reviewed in this work is given in Table 2. Assignments of the specific states responsible for the desorption have been given in the text, and are summarized in more detail elsewhere [10].

Several conclusions can be made based upon the results summarized in this work. They are as follows:

1. In the gas phase, the ESD H^* yield mimics the PSD H^+ yield because electron impact excitation mimics photoionization. However on the surface secondary and backscattered electrons distort this correlation.
2. On the surface, the derivative of the ESD O^+ yield mimics the PSD O^+ yield because the non-resonant ASD mechanism dominates for the O^+ yield. Non-dipole excitations become important near the thresholds.
3. In the DA and RASD mechanisms, the incoming electron provides both the excitation energy and assists in the localization of that energy in the 1h2e and 2h2e states. The photon can only provide for the excitation energy.
4. Secondary and backscattered electrons are important for low threshold desorption processes such as for X^* and X^-, however, the magnitude of this effect in X^+ desorption, where thresholds are higher, is not yet clear.
5. Apparently X^- desorption can result from 1h2e and 2h2e states, X^* from 1h2e, 2h2e, and 2h1e states, and X^+ from 2h1e and 2h

states. Thus as one might intuitively expect, X^- generally results from neutral and negatively charged states, X^* from neutral and singly ionized states, and X^+ from singly or doubly ionized states.

6. Several different mechanisms are responsible for desorption of X^-, X^*, and X^+ from the surface as reviewed in Tables 1 and 2. This study indicates that X^- desorption is an excellent area for study for three reasons: 1) X^- desorption yields appear to be dominated by resonant ESD processes, thus X^- yields are easier to interpret quantitatively than non-resonant ESD X^+ yields; 2) ESD X^- yields are about as straightforward as PSD X^+ yields, but they do not require use of a synchrotron for measurement; 3) X^* yields appear to have contributions from resonant and nonresonant mechanisms making them more complex to interpret, and X^* and $X^\bullet$ are difficult to observe experimentally.

Acknowledgements It is a pleasure to acknowledge helpful discussions with V.M. Bermudez, M.A. Hoffbauer, and F.L. Hutson. This work was supported by the Office of Naval Research.

References

1. "Desorption Induced by Electronic Transitions", N.H. Tolk, M.M. Traum, J.C. Tully, and T.E. Madey, eds., Springer Ser. Chem. Phys., Vol. 24 (Springer-Verlag, Heidelberg, 1983) and references therein.
2. T.E. Madey, D.E. Ramaker, and R. Stockbauer, Ann. Rev. Phys. Chem. 35, 215 (1984).
3. M.L. Knotek, Physics Today 37(9), 24 (1984).
4. D.E. Ramaker, Chem. Phys. 80, 183 (1983).
5. D.E. Ramaker, J. Chem. Phys. 28, 2998 (1983); J. Vac. Sci. Technol. A1, 1137 (1983).
6. P. Feulner, D. Menzel, H.J. Kreuzer, and Z.W. Gorter, Phys. Rev. Lett. 53, 671 (1984).
7. R.H. Stulen, J. Vac. Sci. Technol. A2, 1051 (1984).
8. V.M. Bermudez and M.A. Hoffbauer, Phys. Rev. B30, 1125 (1984).
9. Z.X. Liu and D. Lichtman, Surf. Sci. 114, 287 (1982).
10. D.E. Ramaker, to be published.
11. J.C. Tully, Ref. 1, p. 31.
12. D.E. Ramaker, Ref. 1, p. 70.
13. D. Menzel and R. Gomer, J. Chem. Phys. 41, 3311 (1964); P.A. Redhead, Can. J. Phys. 42, 886 (1964).
14. P. Antoniewicz, Phys. Rev. B21, 3811 (1980).
15. Q.J. Zhang and R. Gomer, Surf. Sci. 109, 567 (1981); Q.J. Zhang, R. Gomer, and R.D. Bowman, Surf. Sci. 129, 535 (1983).
16. M.L. Knotek and P.J. Feibelmann, Phys. Rev. Lett. 40, 964 (1978); Surf. Sci. 90, 78 (1979); Phys. Rev. B18, 6531 (1978).
17. D.E. Ramaker, C.T. White, and J.S. Murday, J. Vac. Sci. Technol. 18, 748 (1981); Phys. Lett. A89, 211 (1982).
18. D.E. Ramaker, Phys. Rev. B21, 4608 (1980); B.I. Dunlap, F.L. Hutson, and D.E. Ramaker, J. Vac. Sci. Technol. 18, 556 (1981).
19. D.R. Jennison and D. Emin, Phys. Rev. Lett. 51, 1390 (1983).
20. C.I.M. Beenakker, F.J. de Heer, H.B. Krop, and G.R. Mohlmann, Chem. Phys. 6, 445 (1974).
21. K.H. Tan, C.E. Brion, Ph.E. Van der Leeuw, and M.J. Van der Wiel, Chem. Phys. 29, 299 (1978).

22. R.B. Cairns, H. Harrison, and R.I. Schoen, J. Chem. Phys. 55, 4886 (1971).
23. N. Kouchi, K. Ito, Y. Hatano, N. Oda, and T. Tsuboi, Chem. Phys. 36, 239 (1979).
24. K. Becker, B. Stumpf, and G. Schulz, Chem. Phys. 53, 31 (1980).
25. C.R. Claydon, G.A. Segal, and H.S. Taylor, J. Chem. Phys. 54, 3799 (1971).
26. K. Becker, B. Stumpf, and G. Schulz, Chem. Phys. Lett. 73, 102 (1980).
27. R.A. Rosenberg, V. Rehn, V.O. Jones, A.K. Green, C.C. Parks, G. Loubiel, and R.H. Stulen, Chem. Phys. Lett. 80, 488 (1981).
28. E. Bertel, D.E. Ramaker, R.L. Kurtz, R. Stockbauer, and T.E. Madey, submitted for publication.
29. R.H. Prince, G.N. Sears, and F.J. Morgan, J. Chem. Phys. 64, 3978 (1976).
30. M. Watanabe, H. Kitamura, and Y. Nakai, in "VUV Radiation Physics", eds., E.E. Koch, R. Haensel, and C. Kunz (Pergamon Press, New York, 1974) p. 70.
31. D. Rapp and D.P. Briglia, J. Chem. Phys. 43, 1480 (1965).
32. G.J. Schulz, Rev. Mod. Phys. 45, 423 (1973).
33. F.L. Hutson, D.E. Ramaker, V.M. Bermudez, and M.A. Hoffbauer, to be published in J. Vac. Sci. Technol.
34. M.L. Knotek, V.O. Jones, and V. Rehn, Phys. Rev. Lett. 43, 300 (1979).
35. M.L. Knotek, Surf. Sci. 101, 334 (1980).
36. R.L. Stockbauer, D.M. Hanson, S.A. Flodstrom, and T.E. Madey, J. Vac. Sci. Technol. 20, 562 (1982); Phys. Rev. B26, 1885 (1982).
37. L.A. Grunes, R.D. Leapman, C.N. Wilker, R. Hoffman, and A.B. Kunz, Phys. Rev. B25, 7157 (1982).
38. T. Kawai, M. Tsukada, H. Adachi, C. Satoko, and T. Sakata, Surf. Sci. 81, L640 (1979).
39. E. Bertel, R. Stockbauer, and T.E. Madey, Surf. Sci. 141, 355 (1984).
40. F.A. Riddoch and M. Jaros, J. Phys. C: Solid St. Phys. 13, 6181 (1980); M. Jaros, F.A. Riddoch, and L.D. Lian, J. Phys. C: Solid St. Phys. 16, L733 (1983).
41. J.E. Demuth, D. Schmeisser, and Ph. Avouris, Phys. Rev. Lett. 47, 1166 (1981).
42. E. Bertel, R. Stockbauer, R.L. Kurtz, D.E. Ramaker, and T.E. Madey, to be published.
43. P.H. Dawson and M.L. Den Boer, Surf. Sci. 122, 588 (1982).
44. T.E. Madey, R. Stockbauer, J.F. van der Veen, and D.E. Eastman, Phys. Rev. Lett. 45, 187 (1980).
45. R. Jaeger, J. Stohr, J. Feldhaus, S. Brennan, and D. Menzel, Phys. Rev. B23, 2102 (1981).
46. F.P. Netzer, G. Strasser, and J.A.D. Matthew, Phys. Rev. Lett. 51, 211 (1983).
47. D.A. Shirley, Phys. Rev. B5, 4709 (1972).

(16)

DL/413/83/01
056/413-2

ABSTRACTS DISTRIBUTION LIST, 056/625/629

Dr. R. G. Wallis
Department of Physics
University of California
Irvine, California 92664

Dr. D. Ramaker
Chemistry Department
George Washington University
Washington, D.C. 20052

Dr. J. C. Hemminger
Chemistry Department
University of California
Irvine, California 92717

Dr. T. F. George
Chemistry Department
University of Rochester
Rochester, New York 14627

Dr. G. Rubloff
IBM
Thomas J. Watson Research Center
P.O. Box 218
Yorktown Heights, New York 10598

Dr. Horia Metiu
Chemistry Department
University of California
Santa Barbara, California 93106

Captain Lee Myers
AFOSR/NC
Bollig AFB
Washington, D.C. 20332

Dr. J. T. Keiser
Department of Chemistry
University of Richmond
Richmond, Virginia 23173

Dr. Roald Hoffmann
Department of Chemistry
Cornell University
Ithaca, New York 14853

Dr. J. E. Jensen
Hughes Research Laboratory
3011 Malibu Canyon Road
Malibu, California 90265

Dr. J. H. Weaver
Department of Chemical Engineering
and Materials Science
University of Minnesota
Minneapolis, Minnesota 55455

Dr. R. W. Plummer
Department of Physics
University of Pennsylvania
Philadelphia, Pennsylvania 19104

Dr. E. Yeager
Department of Chemistry
Case Western Reserve University
Cleveland, Ohio 41106

Dr. N. Winograd
Department of Chemistry
Pennsylvania State University
University Park, Pennsylvania 16802

Dr. G. D. Stein
Mechanical Engineering Department
Northwestern University
Evanston, Illinois 60201

Dr. A. Steckl
Department of Electrical and
Systems Engineering
Rensselaer Polytechnic Institute
Troy, NewYork 12181

Dr. G. H. Morrison
Department of Chemistry
Cornell University
Ithaca, New York 14853

Dr. P. Hansma
Physics Department
University of California
Santa Barbara, California 93106

Dr. J. Baldeschwieler
California Institute of Technology
Division of Chemistry
Pasadena, California 91125

Dr. W. Goddard
California Institute of Technology
Division of Chemistry
Pasadena, California 91125

Dr. W. Knauer
Hughes Research Laboratory
3011 Malibu Canyon Road
Malibu, California 90265

Dr. C. B. Harris
Department of Chemistry
University of California
Berkeley, California 94720

(17)

DL/413/83/01
056/413-2

ABSTRACTS DISTRIBUTION LIST, 056/625/629

Dr. F. Carter
Code 6132
Naval Research Laboratory
Washington, D.C. 20375

Dr. Richard Colton
Code 6112
Naval Research Laboratory
Washington, D.C. 20375

Dr. Dan Pierce
National Bureau of Standards
Optical Physics Division
Washington, D.C. 20234

Dr. R. Stanley Williams
Department of Chemistry
University of California
Los Angeles, California 90024

Dr. R. P. Messmer
Materials Characterization Lab.
General Electric Company
Schenectady, New York 22217

Dr. Robert Gomer
Department of Chemistry
James Franck Institute
5640 Ellis Avenue
Chicago, Illinois 60637

Dr. Ronald Lee
R301
Naval Surface Weapons Center
White Oak
Silver Spring, Maryland 20910

Dr. Paul Schoen
Code 5570
Naval Research Laboratory
Washington, D.C. 20375

Dr. John T. Yates
Department of Chemistry
University of Pittsburgh
Pittsburgh, Pennsylvania 15260

Dr. Richard Greene
Code 5230
Naval Research Laboratory
Washington, D.C. 20375

Dr. L. Kesmodel
Department of Physics
Indiana University
Bloomington, Indiana 47403

Dr. K. C. Janda
California Institute of Technology
Division of Chemistry and Chemical
Engineering
Pasadena, California 91125

Dr. E. A. Irene
Department of Chemistry
University of North Carolina
Chapel Hill, Northc Carolina 27514

Dr. Adam Heller
Bell Laboratories
Murray Hill, New Jersey 07974

Dr. Martin Fleischmann
Department of Chemistry
Southampton University
Southampton SO9 5NH
Hampshire, England

Dr. John W. Wilkins
Cornell University
Laboratory of Atomic and
Solid State Physics
Ithaca, New York 14853

Dr. Richard Smardzewski
Code 6130
Naval Research Laboratory
Washington, D.C. 20375

Dr. H. Tachikawa
Chemistry Department
Jackson State University
Jackson, Mississippi 39217

(18)

DL/413/83/01
056/413-2

ABSTRACTS DISTRIBUTION LIST, 056/625/629

Dr. G. A. Somorjai
Department of Chemistry
University of California
Berkeley, California 94720

Dr. J. Murday
Naval Research Laboratory
Surface Chemistry Division (6170)
455 Overlook Avenue, S.W.
Washington, D.C. 20375

Dr. J. B. Hudson
Materials Division
Rensselaer Polytechnic Institute
Troy, New York 12181

Dr. Theodore E. Madey
Surface Chemistry Section
Department of Commerce
National Bureau of Standards
Washington, D.C. 20234

Dr. J. E. Demuth
IBM Corporation
Thomas J. Watson Research Center
P.O. Box 218
Yorktown Heights, New York 10598

Dr. M. G. Lagally
Department of Metallurgical
and Mining Engineering
University of Wisconsin
Madison, Wisconsin 53706

Dr. R. P. Van Duyne
Chemistry Department
Northwestern University
Evanston, Illinois 60637

Dr. J. M. White
Department of Chemistry
University of Texas
Austin, Texas 78712

Dr. D. E. Harrison
Department of Physics
Naval Postgraduate School
Monterey, California 93940

Dr. W. Kohn
Department of Physics
University of California, San Diego
La Jolla, California 92037

Dr. R. L. Park
Director, Center of Materials
Research
University of Maryland
College Park, Maryland 20742

Dr. W. T. Peria
Electrical Engineering Department
University of Minnesota
Minneapolis, Minnesota 55455

Dr. Keith H. Johnson
Department of Metallurgy and
Materials Science
Massachusetts Institute of Technology
Cambridge, Massachusetts 02139

Dr. S. Sibener
Department of Chemistry
James Franck Institute
5640 Ellis Avenue
Chicago, Illinois 60637

Dr. Arold Green
Quantum Surface Dynamics Branch
Code 3817
Naval Weapons Center
China Lake, California 93555

Dr. A. Wold
Department of Chemistry
Brown University
Providence, Rhode Island 02912

Dr. S. L. Bernasek
Department of Chemistry
Princeton University
Princeton, New Jersey 08544

Dr. P. Lund
Department of Chemistry
Howard University
Washington, D.C. 20059

DL/413/83/01
GEN/413-2

TECHNICAL REPORT DISTRIBUTION LIST, GEN

	No. Copies
Office of Naval Research Attn: Code 413 800 N. Quincy Street Arlington, Virginia 22217	2
Dr. Bernard Douda Naval Weapons Support Center Code 5042 Crane, Indiana 47522	1
Commander, Naval Air Systems Command Attn: Code 310C (H. Rosenwasser) Washington, D.C. 20360	1
Naval Civil Engineering Laboratory Attn: Dr. R. W. Drisko Port Hueneme, California 93401	1
Defense Technical Information Center Building 5, Cameron Station Alexandria, Virginia 22314	12
DTNSRDC Attn: Dr. G. Bosmajian Applied Chemistry Division Annapolis, Maryland 21401	1
Dr. William Tolles Superintendent Chemistry Division, Code 6100 Naval Research Laboratory Washington, D.C. 20375	1
Dr. David Young Code 334 NORDA NSTL, Mississippi 39529	1
Naval Weapons Center Attn: Dr. A. B. Amster Chemistry Division China Lake, California 93555	1
Scientific Advisor Commandant of the Marine Corps Code RD-1 Washington, D.C. 20380	1
U.S. Army Research Office Attn: CRD-AA-IP P.O. Box 12211 Research Triangle Park, NC 27709	1
Mr. John Boyle Materials Branch Naval Ship Engineering Center Philadelphia, Pennsylvania 19112	1
Naval Ocean Systems Center Attn: Dr. S. Yamamoto Marine Sciences Division San Diego, California 91232	1

END

FILMED

1-86

DTIC